

## THE ELM SURVEY. VI. ELEVEN NEW DOUBLE DEGENERATES\*

A. GIANNINAS<sup>1,†</sup>, MUKREMIN KILIC<sup>1</sup>, WARREN R. BROWN<sup>2</sup>, PAUL CANTON<sup>1,†</sup>, AND SCOTT J. KENYON<sup>2</sup>

<sup>1</sup>Homer L. Dodge Department of Physics and Astronomy, University of Oklahoma, 440 W. Brooks St., Norman, OK 73019, USA; alexg@nhn.ou.edu and

<sup>2</sup>Smithsonian Astrophysical Observatory, 60 Garden St., Cambridge, MA 02138, USA

*Accepted for publication in the Astrophysical Journal*

### ABSTRACT

We present the discovery of 11 new double degenerate systems containing extremely low-mass white dwarfs (ELM WDs). Our radial velocity observations confirm that all of the targets have orbital periods  $\leq 1$  day. We perform spectroscopic fits and provide a complete set of physical and binary parameters. We review and compare recent evolutionary calculations and estimate that the systematic uncertainty in our mass determinations due to differences in the evolutionary models is small ( $\approx 0.01 M_{\odot}$ ). Five of the new systems will merge due to gravitational wave radiation within a Hubble time, bringing the total number of merger systems found in the ELM Survey to 38. We examine the ensemble properties of the current sample of ELM WD binaries, including the period distribution as a function of effective temperature, and the implications for the future evolution of these systems. We also revisit the empirical boundaries of instability strip of ELM WDs and identify new pulsating ELM WD candidates. Finally, we consider the kinematic properties of our sample of ELM WDs and estimate that a significant fraction of the WDs from the ELM Survey are members of the Galactic halo.

**Keywords:** binaries: close – Galaxy: stellar content – gravitational waves – supernovae: general – techniques: spectroscopic – white dwarfs

### 1. INTRODUCTION

Short period binary white dwarfs (WDs) are the proposed progenitors of transient events such as supernovae Ia, underluminous .Ia, and Ca-rich supernovae, and other exotic systems like AM CVn, R Coronae Borealis (R CrB), and single subdwarf B/O stars (Webbink 1984; Iben & Tutukov 1984; Bildsten et al. 2007; Perets et al. 2010; Solheim 2010; Clayton 2013; Foley 2015). These binary WDs, including the interacting AM CVn systems, are also expected to be excellent gravitational wave sources and the only known verification binaries for the evolved Laser Interferometer Space Antenna (*eLISA*, Amaro-Seoane et al. 2012). The initial searches for short period double WDs have found systems with periods as short as 1.4 h (Moran et al. 1997), but they failed to find a large number of merging binary systems (Napiwotzki et al. 2007).

Low-mass WDs with  $M \sim 0.4 M_{\odot}$  form  $\approx 10\%$  of the WD population in the solar neighborhood (Liebert et al. 2005), and the majority of them are found in binary systems (Marsh et al. 1995; Napiwotzki et al. 2007; Brown et al. 2011a; Debes et al. 2015). This is expected, as the Galaxy is not old enough to produce  $M \leq 0.5 M_{\odot}$  WDs through single star evolution. The youngest WDs in Milky Way’s globular clusters have  $M > 0.5 M_{\odot}$  (Hansen et al. 2007), consistent with this explanation.

Extremely low-mass (ELM) WDs with  $M < 0.3 M_{\odot}$  provide a unique opportunity to significantly enlarge the known population of merging WDs in the Galaxy. The ELM Survey is a targeted search for these WDs in a well defined color and temperature range (Brown et al. 2010, 2012, 2013; Kilic et al. 2010b, 2011, 2012). This survey has so far identified 56 bi-

naries, all with  $P \leq 1$  d, including 33 merger systems and four binaries with  $P < 1$  h. The two shortest period systems, J0651 and J0935 (WD 0931+444), will merge in  $< 1$  Myr and  $< 10$  Myr, respectively (Brown et al. 2011b; Kilic et al. 2014a).

ELM WDs display a variety of photometric effects, including doppler beaming (Shporer et al. 2010), tidal distortions, pulsations, and eclipses. There are currently six eclipsing (Steinfadt et al. 2010; Brown et al. 2011b; Vennes et al. 2011; Parsons et al. 2011; Kilic et al. 2014b; Hallakoun et al. 2015), six pulsating (Hermes et al. 2013a; Kilic et al. 2015), and eight tidally distorted (Hermes et al. 2014) ELM WDs known. The discovery of new ELM WDs, hence, provides new opportunities to improve the mass-radius relation and our understanding of the interior structure of low-mass WDs.

Brown et al. (2012) describe an efficient way to delineate ELM WDs from normal WDs, A stars, and quasars, by targeting a color-selected sample of  $g = 15 - 20$  mag low-mass WD candidates (see Fig. 1 of Brown et al. 2012). Here we extend the target selection to the SDSS Data Release 9 area while continuing to apply the same color selection criteria and provide the first discoveries from this extended survey. Three of our targets, J1130+3855, J1526+0543, and J1617+1310, were previously identified as ELM WDs by Brown et al. (2012) based on single epoch observations. Here we present follow-up radial velocity observations of these three targets, as well as nine newly identified ELM WDs.

We have also been obtaining radial-velocity measurements for candidates from other sources including the Large Sky Area Multi-Object Spectroscopy Telescope (LAMOST, Wang et al. 1996; Cui et al. 2012). Zhao et al. (2013) describe how a number of WDs were identified from the LAMOST data but objects with  $\log g < 7.0$  were rejected as WDs. The spectra of these discarded objects were kindly provided to us by J. K. Zhao (2013, private communication). Based on our fits of these spectra, we identified a number of possible ELM WD candidates including J0308+5140 and J1249+2626. Coincidentally, J1249+2626 lies within the SDSS footprint,

\* Based on observations obtained at the MMT Observatory, a joint facility of the Smithsonian Institution and the University of Arizona.

† Visiting Astronomer, Kitt Peak National Observatory, National Optical Astronomy Observatory, which is operated by the Association of Universities for Research in Astronomy (AURA) under cooperative agreement with the National Science Foundation.

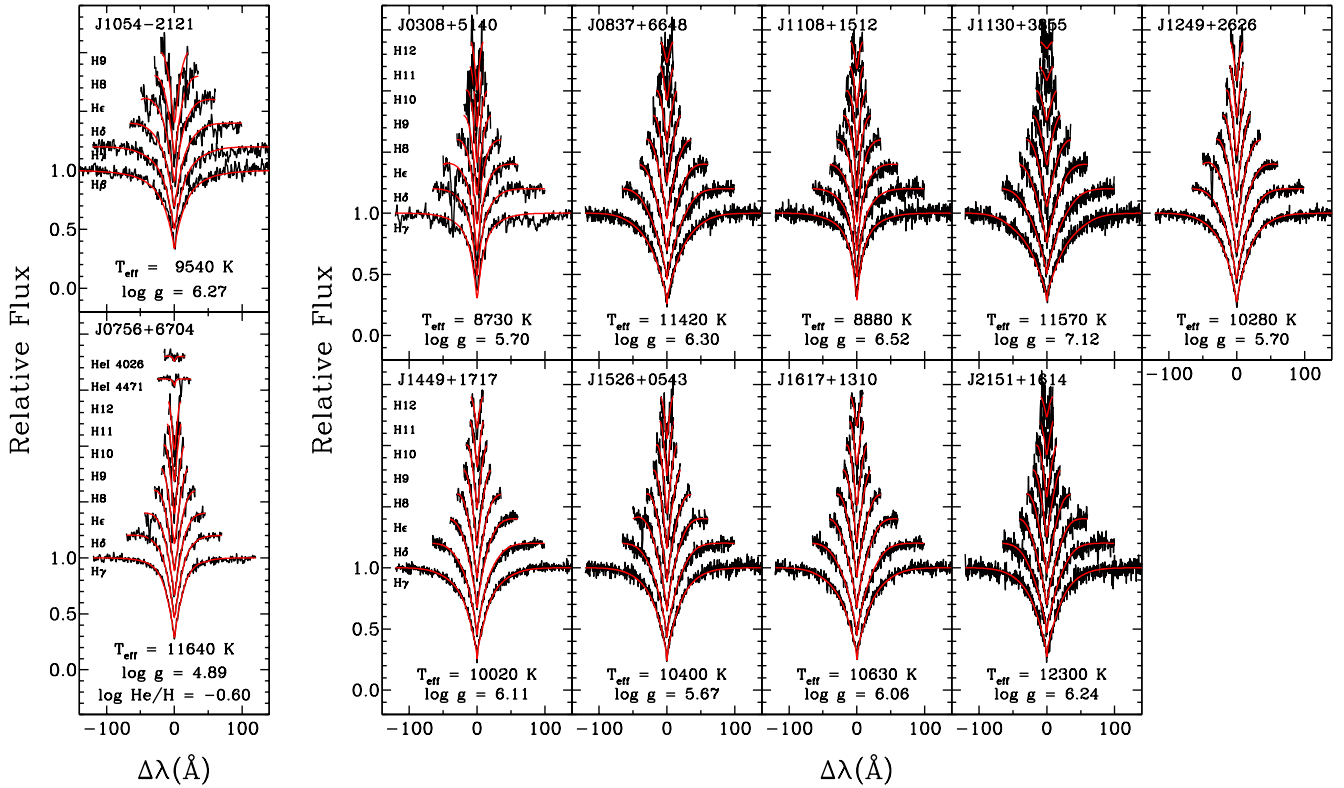


**Figure 1.** 1D model fits (red) to the observed Balmer line profiles (black) for the 11 new ELM WDs binaries. In the right panel, we show fits to 9 ELM WDs, with optical spectra obtained at the MMT and FLWO, using pure H model atmospheres and include the lines from H $\gamma$  (bottom) to H12 (top). We also show model fits for J1054–2121 (left panel, top) whose spectrum was obtained using the Kitt Peak 4 m and includes the lines from H $\beta$  to H9. Finally, fits using a mixed H-He model grid are shown for J0756+6704 (left panel, bottom) where we fit the He I  $\lambda$ 4026 and He I  $\lambda$ 4471 lines in addition to the Balmer lines. Individual spectral lines are offset by a factor of 0.2 for clarity. The best-fit atmospheric parameters are indicated at the bottom of each panel.

however J0308+5140 does not.

Section 2 describes our spectroscopic observations. Section 3 presents the physical and orbital parameters of the eleven new ELM WDs in our survey. The sample characteristics of all 67 binaries in the ELM Survey are discussed in Section 4 and we conclude in Section 5.

## 2. OBSERVATIONS AND MODELLING

### 2.1. Optical Spectroscopy

We used the 6.5m MMT telescope equipped with the Blue Channel spectrograph (Schmidt et al. 1989), the 200-inch Hale telescope equipped with the Double spectrograph (Oke & Gunn 1982), the Kitt Peak National Observatory 4m telescope equipped with the R-C spectrograph, and more recently with KOSMOS (Martini et al. 2014), to obtain spectroscopy of our eleven targets in several observing runs. We operated the Blue Channel, Double, R-C, and KOSMOS spectrographs with the 832 line mm $^{-1}$ , 1200 line mm $^{-1}$ , KPC22B, and b2k gratings, providing wavelength coverages of 3650–4500 Å, 3650–5180 Å, 3700–5170 Å and 3500–6200 Å and spectral resolutions of 1.0 Å, 1.7 Å, 2.2 Å, and 2.0 Å, respectively. We also observed two of the targets with  $g < 17$  mag in queue scheduled time at the 1.5 m FLWO telescope using the FAST spectrograph (Fabricant et al. 1998) with the 600 line mm $^{-1}$  grating, providing 3500–5500 Å wavelength coverage with a spectral resolution of 2.3 Å. The Kitt Peak and Palomar observations were obtained as part of the NOAO programs 2012A-0055, 2012B-0114, 2013A-0276, 2013B-0130, 2014A-0189, and 2015A-0082. The MMT and Hale

observations were obtained at the parallactic angle, but the Kitt Peak and FLWO observations were obtained at a fixed slit angle. A comparison lamp exposure was obtained with every observation. We flux-calibrate using blue spectrophotometric standards (Massey et al. 1988).

We measure radial velocities using the cross-correlation package RVSAO (Kurtz & Mink 1998). Given the differences in wavelength coverage and resolution of the five instruments used in our work, we cross-correlate the observed spectra with the best-fit model WD templates (see §2.2) at the appropriate resolution for each spectrum. The average precision of our measurements ranges from about 10 km s $^{-1}$  to 20 km s $^{-1}$ . We compute best-fit orbital elements using the code of Kenyon & Garcia (1986), which weights each velocity measurement by its associated error. We perform a Monte Carlo analysis to verify the uncertainties in the orbital parameters (see Brown et al. 2012).

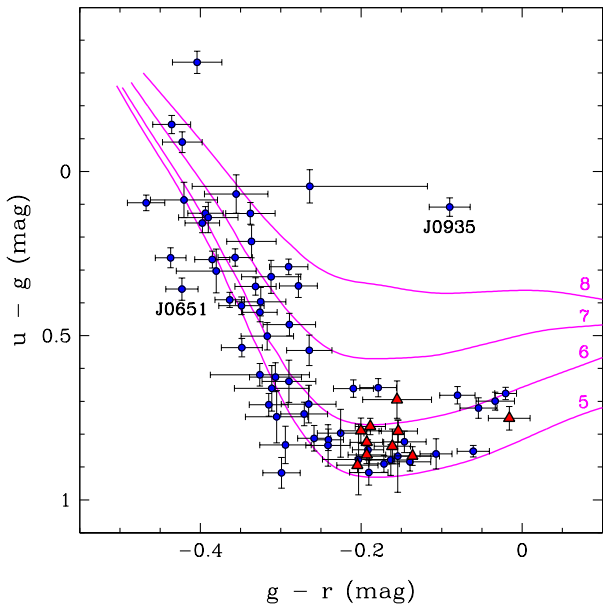
### 2.2. WD Model Atmosphere Analysis

Figure 1 presents the Balmer line profile fits for our 11 new ELM WDs. We use a pure-hydrogen model atmosphere grid covering  $T_{\text{eff}} = 4000 - 35,000$  K and  $\log g = 4.5 - 9.5$  and the spectroscopic technique described in Gianninas et al. (2011, 2014a, and references therein) to fit the Balmer line profiles of each target. The models include the Stark broadening profiles from Tremblay & Bergeron (2009). We fit all of the visible Balmer lines up to H12 in the MMT and Hale data, but we only fit H $\beta$  through H9 for the Kitt Peak data due to the decrease in sensitivity below 3800 Å. The results from different telescopes agree within the errors, but we adopt the values

**Table 1**  
ELM WD Physical Parameters

SDSS	R.A. (h:m:s)	Decl. (d:m:s)	$T_{\text{eff}}$ (K)	$\log g$ ( $\text{cm s}^{-2}$ )	$M_1$ ( $M_{\odot}$ )	$g_0$ (mag)	$M_g$ (mag)	$d$ (kpc)	$\tau_{\text{cool}}$ (Gyr)
J0308+5140	03:08:18.19	+51:40:11.52	$8380 \pm 140$	$5.51 \pm 0.10$	$0.151 \pm 0.024$	$13.049 \pm 0.010$	$8.04 \pm 0.53$	$0.100 \pm 0.025$	$1.128 \pm 0.358$
J0756+6704	07:56:10.71	+67:04:24.69	$11640 \pm 250$	$4.90 \pm 0.14$	$0.181 \pm 0.011$	$16.233 \pm 0.020$	$5.22 \pm 0.46$	$1.597 \pm 0.343$	$0.189 \pm 0.078$
J0837+6648	08:37:08.51	+66:48:37.12	$11400 \pm 240$	$6.31 \pm 0.05$	$0.181 \pm 0.011$	$17.844 \pm 0.019$	$8.83 \pm 0.25$	$0.634 \pm 0.072$	$1.157 \pm 0.123$
J1054-2121	10:54:35.78	-21:21:55.94	$9210 \pm 140$	$6.14 \pm 0.13$	$0.168 \pm 0.011$	$18.487 \pm 0.013$	$9.11 \pm 0.49$	$0.751 \pm 0.169$	$2.649 \pm 0.256$
J1108+1512	11:08:15.51	+15:12:46.74	$8700 \pm 130$	$6.23 \pm 0.06$	$0.167 \pm 0.010$	$18.830 \pm 0.017$	$9.61 \pm 0.28$	$0.698 \pm 0.090$	$3.602 \pm 0.505$
J1130+3855	11:30:17.45	+38:55:50.11	$11430 \pm 190$	$7.12 \pm 0.06$	$0.286 \pm 0.018$	$19.446 \pm 0.021$	$10.34 \pm 0.26$	$0.662 \pm 0.079$	$0.287 \pm 0.055$
J1249+2626	12:49:43.57	+26:26:04.22	$10120 \pm 160$	$5.72 \pm 0.05$	$0.161 \pm 0.010$	$16.566 \pm 0.015$	$7.76 \pm 0.24$	$0.576 \pm 0.064$	$1.541 \pm 0.153$
J1449+1717	14:49:57.15	+17:17:29.33	$9700 \pm 150$	$6.08 \pm 0.05$	$0.168 \pm 0.010$	$17.620 \pm 0.018$	$8.76 \pm 0.25$	$0.591 \pm 0.068$	$2.152 \pm 0.128$
J1526+0543	15:26:51.57	+05:43:35.31	$10290 \pm 190$	$5.69 \pm 0.05$	$0.162 \pm 0.010$	$18.754 \pm 0.020$	$7.63 \pm 0.25$	$1.677 \pm 0.193$	$1.413 \pm 0.150$
J1617+1310	16:17:22.51	+13:10:18.87	$10510 \pm 170$	$6.07 \pm 0.05$	$0.172 \pm 0.010$	$18.602 \pm 0.015$	$8.47 \pm 0.24$	$1.062 \pm 0.117$	$1.626 \pm 0.099$
J2151+1614	21:51:59.21	+16:14:48.72	$12300 \pm 230$	$6.24 \pm 0.06$	$0.176 \pm 0.010$	$16.454 \pm 0.014$	$8.51 \pm 0.24$	$0.387 \pm 0.044$	$0.882 \pm 0.098$

**Notes.** The listed  $T_{\text{eff}}$  and  $\log g$  values are corrected for 3D effects according to Tremblay et al. (2015).



**Figure 2.** Color-color diagram of the WDs in the ELM Survey (blue circles), including 10 of the 11 systems identified in this paper (red triangles). Magenta lines show synthetic colors of WD model sequences with  $T_{\text{eff}} = 30,000 - 7500$  K and  $\log g = 5, 6, 7,$  and  $8$ . The two shortest period detached binary WD systems currently known, J0651 and J0935 (WD 0931+444), are labeled.

from the MMT data (when available) since those spectra have the highest signal-to-noise ratio and resolution, and include all of the higher order Balmer lines.

J0756+6704 also displays the He I  $\lambda 4026$  and He I  $\lambda 4471$  lines in its optical spectrum. In this case, we use a grid of mixed H-He model atmospheres to fit  $T_{\text{eff}}$ ,  $\log g$ , as well as the helium abundance. The measured abundance of  $\log(\text{He}/\text{H}) = -0.60 \pm 0.38$  coupled with the rather low surface gravity of  $\log g = 4.89$  makes it very similar to the mixed H-He ELM WDs analyzed in Gianninas et al. (2014a) and is potentially a sign of a recent shell flash.

We also note the continuing presence of the Ca II  $\lambda 3934$  line in the blue wing of He for all ELM WDs with  $\log g < 6.0$  (Brown et al. 2013; Gianninas et al. 2014a) including J0308+5140, J0756+6704, J1249+2626, J1526+0543 as well

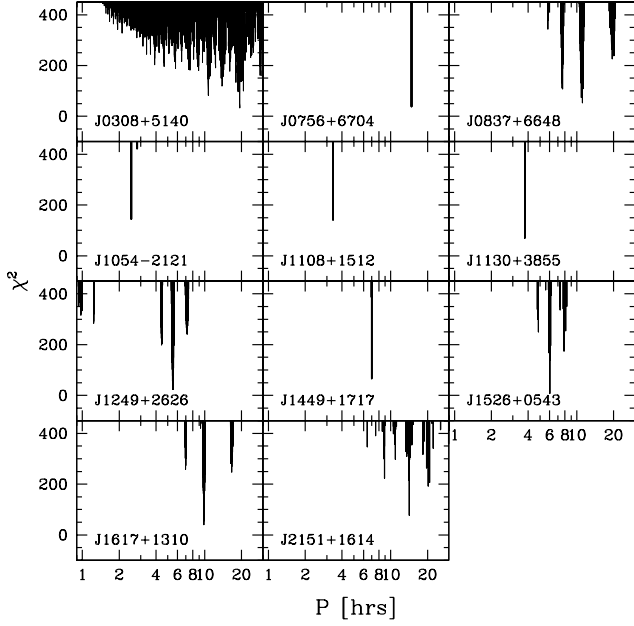
as J1054-2121. Furthermore, in both our spectrum and the SDSS spectrum of J0756+6704, the Mg II  $\lambda 5173-5184$  doublet is clearly visible. The Na D lines are also definitively detected in the SDSS spectrum of J0756 and the LAMOST spectrum of J0308+5140. These features mark J0756+6704 and J0308+5140 as most intriguing systems worthy of a more detailed analysis (e.g. Gianninas et al. 2014a; Hermes et al. 2014). In all cases, the spectral range where the Ca line is present is excluded from both the normalization and fitting procedures.

Table 1 summarizes the measured atmospheric parameters,  $T_{\text{eff}}$  and  $\log g$ . Note that the values listed in Table 1 have been corrected using the new 3D correction functions from Tremblay et al. (2015) and thus differ from those displayed in Figure 1. The corrections have been applied to all targets with  $T_{\text{eff}} \leq 12,000$  K which includes all 11 new ELM WDs save J2151+1614.

Based on the recent evolutionary sequences for ELM WDs by Althaus et al. (2013), we estimate masses ( $M_1$ ), absolute magnitudes ( $M_g$ ), and WD cooling ages ( $\tau_{\text{cool}}$ ) for each object. Given  $M_g$  and the extinction corrected SDSS  $g$ -band magnitude ( $g_0$ ). However, since J0308+5140 is located outside the SDSS footprint, for this object we estimate the  $g$ -band magnitude from The Fourth US Naval Observatory CCD Astrograph Catalog (UCAC4, Zacharias et al. 2013). We also derive distances ( $d$ ) to each object. These are also included in Table 1. All 11 targets have  $T_{\text{eff}} \approx 8000 - 12,000$  K,  $\log g = 4.9 - 7.1$ ,  $M \approx 0.15 - 0.29 M_{\odot}$  and they are located at  $d \approx 0.10 - 1.70$  kpc from the Sun.

Contrary to previous analyses (Gianninas et al. 2014a,b), we do not adopt a systematic uncertainty of  $0.02 M_{\odot}$  for our determination of  $M_1$ . Instead, we propagate the uncertainties in  $T_{\text{eff}}$  and  $\log g$  through our interpolation of the Althaus et al. (2013) model grid after which we add, in quadrature, the systematic uncertainty of  $0.01 M_{\odot}$  (see Section 4.2.1).

Figure 2 shows a color-color diagram of all of the ELM WDs identified in the ELM Survey, including 10 of the 11 systems described in this paper. The latter systems were selected to have  $g-r = -0.2$  to  $0.0$  mag based on the color-selection of Brown et al. (2012). Hence, it is not surprising that they all have temperatures near  $10,000$  K. This figure demonstrates that ELM WDs have colors consistent with the WD model sequences, except J0935 (WD 0931+444), whose photometry is contaminated by an M dwarf (Kilic et al. 2014a).



**Figure 3.** Periodograms for the 11 new ELM WD binaries. The best orbital periods have the smallest  $\chi^2$  values; some binaries are well constrained and some have period aliases.

### 2.2.1. J0308+5140

Fitting the optical spectrum of J0308+5140 required an additional treatment. It is clear from the spectra that J0308+5140 suffers from a considerable amount of reddening, consistent with its Galactic latitude of  $b = -5.67^\circ$ . According to the NASA/IPAC Infrared Science Archive (IRSA) dust maps<sup>1</sup>, the reddening in the direction of J0308+5140 is  $E(B-V) = 0.795$ . Adopting this value for the reddening, we follow the prescription of Seaton (1979) to de-redden the observed spectrum of J0308+5140. The slope of the corrected spectrum is in excellent agreement with the slope of the spectroscopic solution. Consequently, we adopt an extinction of  $A_g = 3.014$  from IRSA to correct the  $g$ -band magnitude of J0308+5140 from UCAC4 (i.e.  $g = 16.063$ ) to get  $g_0 = 13.049$ , as listed in Table 1.

## 3. ORBITAL PARAMETERS

Figure 3 shows the periodograms for our 11 targets. All of our targets have a well defined minimum  $\chi^2$  in the periodograms and the period is constrained to  $P \leq 1$  d in all cases. Furthermore, to obtain a  $p$ -value of  $p = 0.01$  with four degrees of freedom requires a  $\Delta\chi^2 \geq 13.3$ , with respect to the minimum  $\chi^2$  (Press et al. 1986). This criterion is met by all the new ELM WD binaries. Thus, the orbital periods we determine are statistically significant at the 99% confidence level.

Table 2 and Figure 4 present the best-fit orbital parameters and the radial velocity curves, respectively. Table 2 lists the orbital period ( $P$ ), radial velocity semi-amplitude ( $K$ ), systemic velocity ( $\gamma$ ), the mass function, the minimum secondary mass ( $M_2$ ) assuming  $i = 90^\circ$ , the secondary mass assuming  $i = 60^\circ$ , the maximum gravitational wave merger time ( $\tau_{\text{merge}}$ ), the orbital separation ( $a$ ) and finally, the gravitational wave strain ( $\log h$ ).

Our targets show radial velocity variations with orbital pe-

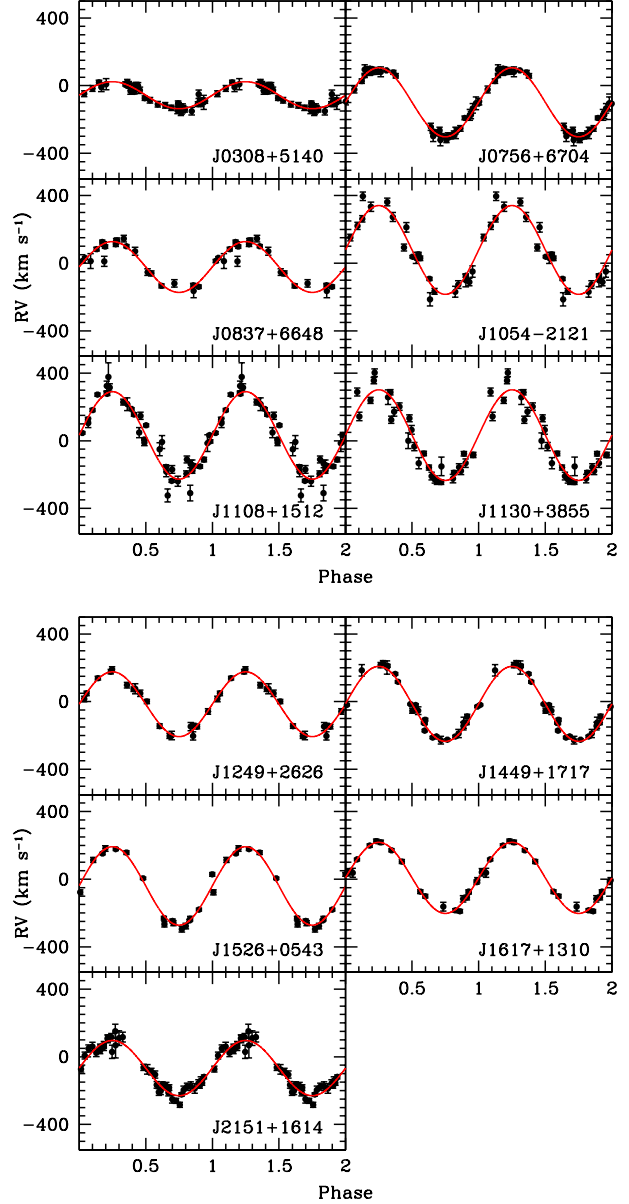


**Figure 4.** Observed velocities phased to the best-fit orbits (red) for the 11 new ELM WD binaries.

riods of  $P \approx 3\text{--}19$  h and semi-amplitudes of  $K \approx 80$  to  $\approx 285$  km s<sup>-1</sup>. The systemic velocities range from  $\gamma \approx -100$  to  $\approx 100$  km s<sup>-1</sup>. We note that the systemic velocities do not include the corrections for the WDs' gravitational redshift, which is a few km s<sup>-1</sup>.

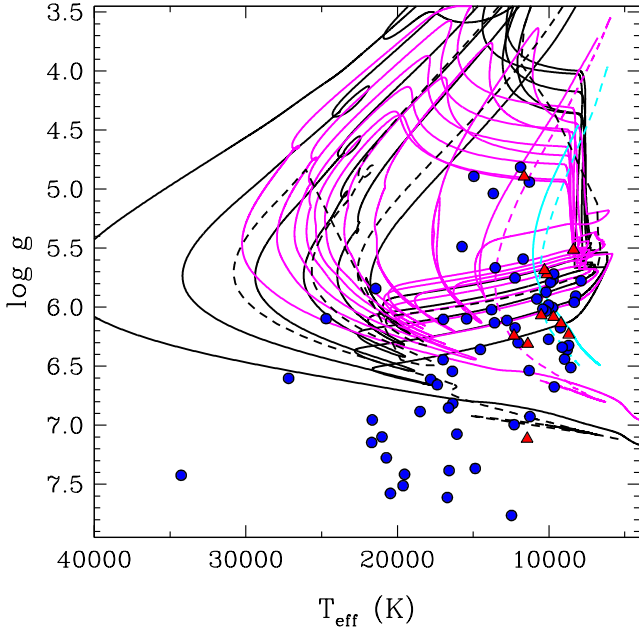
The minimum mass companions to these 11 ELM WDs range from  $0.16 M_\odot$  to  $0.82 M_\odot$ . Based on the mass function, the probability of a  $1.4\text{--}3.0 M_\odot$  neutron star companion ranges from 2% to a maximum of 20% for the companion of J0756+6704. These percentages are quite low and it is unlikely that any of these 11 new ELM WDs have neutron star companions. These probabilities agree with the recent studies of Andrews et al. (2014) and Boffin (2015) whose results imply that neutron star companions to ELM WDs should be rare.

It is also unlikely that the total masses for any of these new systems is above the Chandrasekhar mass limit. Assuming

<sup>1</sup> <http://irsa.ipac.caltech.edu/applications/DUST/>

**Table 2**  
 ELM WD Binary Parameters

SDSS	$P$ (days)	$K$ (km s <sup>-1</sup> )	$\gamma$ (km s <sup>-1</sup> )	Mass Function ( $M_{\odot}$ )	$M_2$ ( $M_{\odot}$ )	$M_{2,i=60^{\circ}}$ ( $M_{\odot}$ )	$\tau_{\text{merge}}$ (Gyr)	$a$ ( $R_{\odot}$ )	$\log h$
J0308+5140	$0.80590 \pm 0.00038$	$78.9 \pm 2.7$	$-56.8 \pm 1.8$	$0.041 \pm 0.004$	$\geq 0.16 \pm 0.02$	$0.20 \pm 0.03$	...	$2.46 \pm 0.12$	-22.57
J0756+6704	$0.61781 \pm 0.00002$	$204.2 \pm 1.6$	$-98.7 \pm 1.3$	$0.545 \pm 0.013$	$\geq 0.82 \pm 0.03$	$1.13 \pm 0.04$	...	$3.05 \pm 0.04$	-23.05
J0837+6648	$0.46329 \pm 0.00005$	$150.3 \pm 3.0$	$-22.4 \pm 2.3$	$0.163 \pm 0.010$	$\geq 0.37 \pm 0.02$	$0.48 \pm 0.03$	...	$2.06 \pm 0.04$	-22.85
J1054-2121	$0.10439 \pm 0.00655$	$261.1 \pm 7.1$	$94.3 \pm 4.5$	$0.193 \pm 0.028$	$\geq 0.39 \pm 0.05$	$0.52 \pm 0.06$	$\leq 1.452$	$0.77 \pm 0.06$	-22.49
J1108+1512	$0.12310 \pm 0.00867$	$256.2 \pm 3.7$	$44.5 \pm 2.4$	$0.214 \pm 0.024$	$\geq 0.42 \pm 0.04$	$0.56 \pm 0.05$	$\leq 2.143$	$0.87 \pm 0.07$	-22.48
J1130+3855	$0.15652 \pm 0.00001$	$284.0 \pm 4.9$	$24.5 \pm 3.6$	$0.371 \pm 0.019$	$\geq 0.72 \pm 0.04$	$0.96 \pm 0.05$	$\leq 1.652$	$1.23 \pm 0.02$	-22.14
J1249+2626	$0.22906 \pm 0.00112$	$191.6 \pm 3.9$	$-15.5 \pm 2.4$	$0.167 \pm 0.011$	$\geq 0.35 \pm 0.02$	$0.47 \pm 0.03$	$\leq 13.242$	$1.26 \pm 0.03$	-22.65
J1449+1717	$0.29075 \pm 0.00001$	$228.5 \pm 3.2$	$3.9 \pm 3.0$	$0.359 \pm 0.015$	$\geq 0.59 \pm 0.03$	$0.81 \pm 0.04$	...	$1.69 \pm 0.03$	-22.54
J1526+0543	$0.25039 \pm 0.00001$	$231.9 \pm 2.3$	$-39.8 \pm 1.8$	$0.324 \pm 0.010$	$\geq 0.54 \pm 0.02$	$0.74 \pm 0.02$	$\leq 12.087$	$1.49 \pm 0.02$	-22.99
J1617+1310	$0.41124 \pm 0.00086$	$210.1 \pm 2.8$	$7.7 \pm 2.0$	$0.395 \pm 0.017$	$\geq 0.64 \pm 0.03$	$0.87 \pm 0.04$	...	$2.17 \pm 0.04$	-22.86
J2151+1614	$0.59152 \pm 0.00008$	$163.3 \pm 3.1$	$-67.0 \pm 2.3$	$0.267 \pm 0.015$	$\geq 0.49 \pm 0.03$	$0.66 \pm 0.04$	...	$2.59 \pm 0.05$	-22.61


**Figure 5.** Location in the  $T_{\text{eff}} - \log g$  plane of the 11 new ELM WDs presented in this paper (red triangles) along with the complete ELM Survey sample (blue circles). Also plotted are evolutionary tracks from Althaus et al. (2013) (solid lines) and Istrate et al. (2014) (dashed lines) for  $0.165 M_{\odot}$  (cyan),  $0.187 M_{\odot}$  (magenta), and  $0.239 M_{\odot}$  (black).

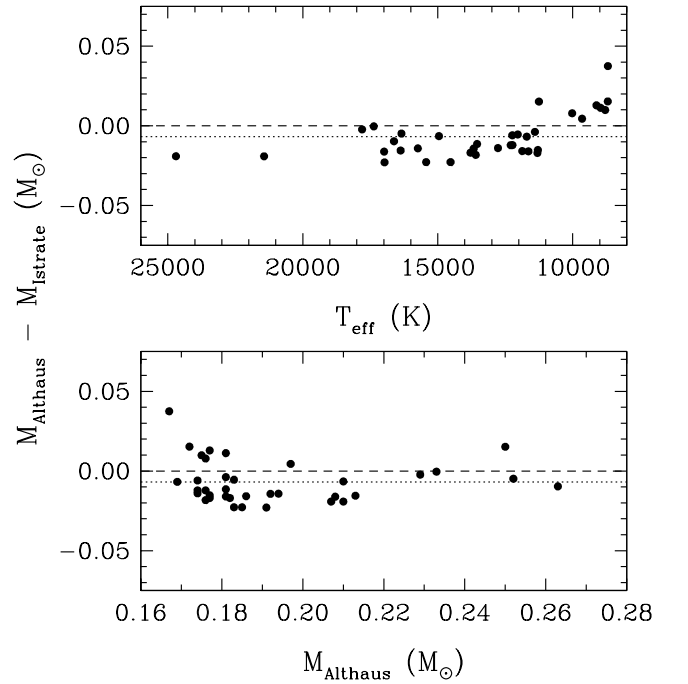
an average inclination of  $i = 60^{\circ}$ , the binaries with the highest total system mass are J0756+6704 and J1130+3855 with  $M_{\text{tot}} = 1.31 M_{\odot}$  and  $1.25 M_{\odot}$ , respectively.

Our sample also includes five new merger systems (J1054-2121, J1108+1512, J1130+3855, J1249+2626, J1526+0543). The quickest to merge will be J1054-2121 with  $\tau_{\text{merge}} = 1.452$  Gyr. However, the gravitational wave strains of these systems are not strong enough to be detected by *eLISA* (see Figure 12 of Gianninas et al. 2014a).

## 4. DISCUSSION

### 4.1. Eleven New Binary WD Systems

With these 11 new discoveries, and including the pulsating ELM WDs published by Hermes et al. (2013b,a), and the discoveries presented in Kilic et al. (2014a,b) and


**Figure 6.** Difference in the primary mass as determined using the models from Althaus et al. (2013,  $M_{\text{Althaus}}$ ) and Istrate et al. (2014,  $M_{\text{Istrate}}$ ) plotted as a function of  $T_{\text{eff}}$  (top) and  $M_{\text{Althaus}}$  (bottom). The dotted line denotes the average difference.

Gianninas et al. (2014b), the ELM Survey has found a total of 73 ELM WDs of which 67 are in detached, double-degenerate binaries; 38 of the binaries will merge within a Hubble time. Counting only six systems where no significant radial velocity variability has been detected, 92% of the ELM Survey targets are formally members of compact ( $P < 1$  d) binary systems. In addition to the results listed in Tables 1 and 2, we provide, for completeness, the physical and binary parameters for the entire ELM Survey sample in Tables 4 and 5 of the Appendix. Note that for ELM WDs with  $T_{\text{eff}} < 12,000$  K, the atmospheric parameters have been adjusted using the 3D corrections from Tremblay et al. (2015).

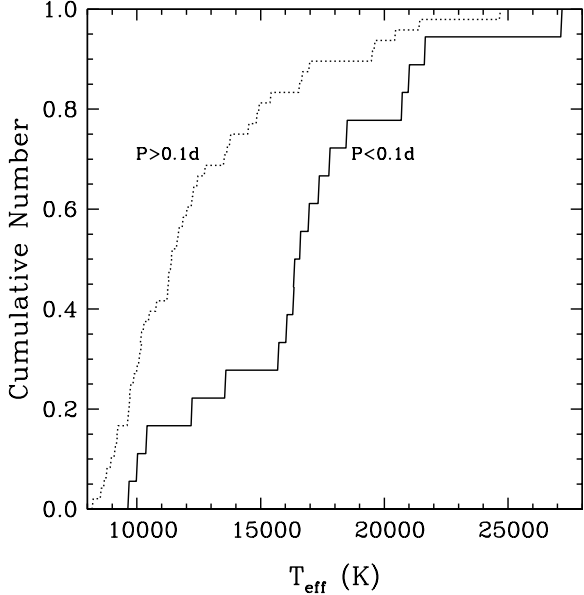


**Figure 7.** Cumulative distribution as a function of  $T_{\text{eff}}$  for ELM WDs with  $P < 0.1$  d (solid line) and  $P > 0.1$  d (dotted line).

#### 4.2. The ELM WD Sample

##### 4.2.1. Comparison of Evolutionary Models

In Table 1 we adopt masses derived from the evolutionary sequences for He-core WDs of Althaus et al. (2013). However, new evolutionary sequences appropriate for He-core ELM WDs have recently been published by Istrate et al. (2014). Due to the importance of obtaining accurate masses in order to correctly predict the final merger products of ELM WD binaries, it is important to explore these new evolutionary calculations.

One of the major differences between the Althaus et al. (2013) and Istrate et al. (2014) models are the initial assumptions with regards to the progenitors and companions of the eventual ELM WDs. All of the Althaus et al. (2013) models assume a  $1.0 M_{\odot}$  progenitor for the ELM WD and are evolved in a binary with a  $1.4 M_{\odot}$  neutron star companion. In contrast, the Istrate et al. (2014) models assume a range of progenitor masses (from  $1.2$  to  $1.6 M_{\odot}$ ) as well as a range of neutron star masses (from  $1.3$  to  $1.75 M_{\odot}$ ) to produce the full range of ELM WD masses in their model grid. As we will demonstrate, both approaches yield similar ELM WD masses. However, as we mentioned in Section 3, neutron star companions are unlikely in most of these systems. Consequently, it would be useful to have evolutionary tracks computed for ELM WD binaries with massive WD companions instead to provide additional insight into the final ELM WD masses.

In Figure 5, we plot the location of all ELM WDs from the ELM Survey sample in the  $T_{\text{eff}} - \log g$  plane. In addition, we plot a selection of evolutionary tracks from both Althaus et al. (2013) and Istrate et al. (2014). In order to make the most direct comparison possible, we have chosen a set of three representative evolutionary tracks corresponding to final ELM WD masses of  $0.165 M_{\odot}$ ,  $0.187 M_{\odot}$ , and  $0.239 M_{\odot}$ .

The results in Figure 5 demonstrate that there are significant differences between the two sets of evolutionary tracks. Most notably, the Istrate et al. (2014) models predict considerably fewer shell flashes than the Althaus et al. (2013) tracks. This is most clearly seen in the  $0.187 M_{\odot}$  tracks (magenta) where the Istrate model predicts no shell flashes while the equivalent

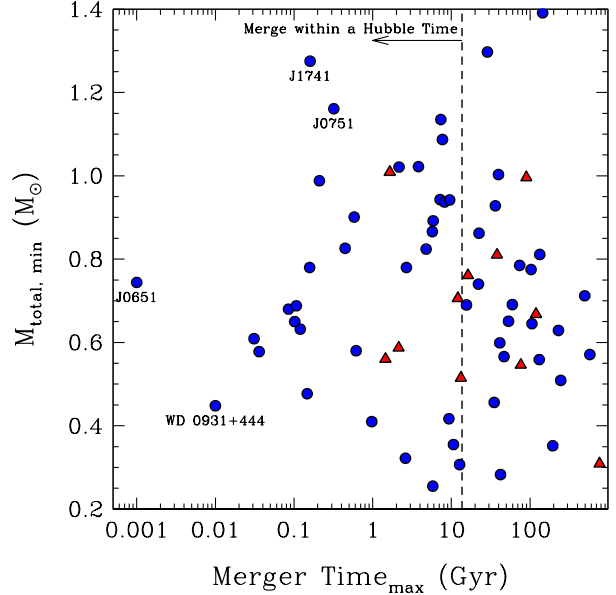


**Figure 8.** Plot of the minimum total mass as a function of the maximum merger time for the entire ELM Survey sample (blue circles) with the 11 new binaries from this paper (red triangles).

Althaus model undergoes a series of shell flashes. Indeed, the Althaus models assume  $Z = 0.01$  while the Istrate models assume  $Z = 0.02$ . Since the maximum mass for which flashes occur increases with lower metallicity (Nelson et al. 2004), it is not surprising that the Althaus models predict a greater number of shell flashes and for a broader range of masses.

Despite these significant differences, the most important question is whether or not the models yield the same masses for a given  $T_{\text{eff}}$  and  $\log g$ . We have chosen a set of nine models from the grid of Istrate et al. (2014) to compute masses. To greatly simplify the calculation, we consider only the final cooling portion of the evolutionary tracks. In Figure 6 we plot the difference in masses derived from the two model grids as a function of  $T_{\text{eff}}$  and  $M_{\text{Althaus}}$ . Figure 6 demonstrates that the Althaus & Istrate models yield very similar masses. The average difference is  $\approx 0.01 M_{\odot}$  with an overall scatter of roughly the same magnitude. Consequently, we adopt an uncertainty of  $0.01 M_{\odot}$  as the systematic error due to uncertainties in the evolutionary models. This is equivalent to an error of  $\approx 5\%$  in mass. In contrast, the mean error in mass due to uncertainties in the atmospheric parameters,  $T_{\text{eff}}$  and  $\log g$ , is  $\approx 0.006 M_{\odot}$  which is  $\approx 3\%$ . Therefore, the error in our mass estimates is dominated by the systematic uncertainties from the evolutionary models.

##### 4.2.2. The Period Distribution of Binary WDs

In Figure 7 we plot the cumulative distributions, as a function of  $T_{\text{eff}}$ , for the 18 systems with  $P < 0.1$  d and the 49 systems with  $P > 0.1$  d. We see that the majority of systems with  $P > 0.1$  d are found with  $T_{\text{eff}} \lesssim 15,000$  K.

To determine if the two distributions are statistically independent, we perform the two-sample Kolmogorov-Smirnov (K-S) test. The K-S statistic,  $D_{n,n'}$ , is defined as the largest difference between the cumulative distributions functions and can be expressed as

$$D_{n,n'} = \sup_x |F_{1,n}(x) - F_{2,n'}(x)|$$

where  $F_{1,n}(x)$  and  $F_{2,n'}(x)$  represent the  $P > 0.1$  d and  $P < 0.1$  d

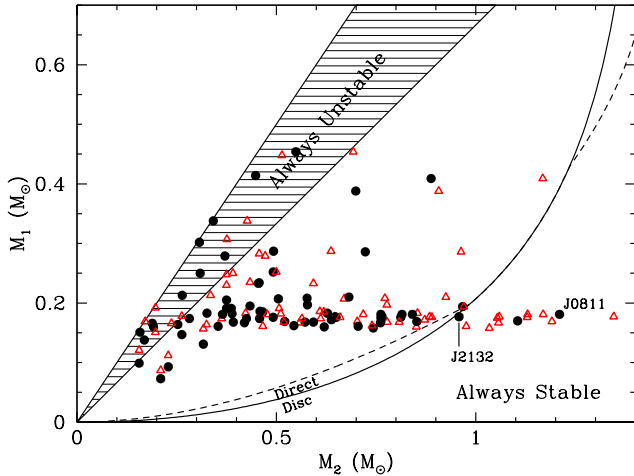


**Figure 9.** Plot of  $M_1$  vs.  $M_2$  for the entire ELM sample. Black points represent  $M_{2,\min}$  while the red triangles assume  $M_{2,i=60^\circ}$ . The majority of the ELM WD binaries lie in the region between the regions of stable and unstable mass transfer.

distributions, respectively. For the given distributions in Figure 7, we determine a K-S statistic of  $D_{n,n'} = 0.5590$  and a  $p$ -value of  $p = 0.0002$ . Based on this result, we can reject the null hypothesis at the  $\alpha = 0.01$  significance level. However, the K-S test is not always sensitive enough to determine if two distributions are indeed independent. This is because, by definition, the distributions converge to 0 and 1 at the ends. The Anderson-Darling (A-D) test is more useful in such situations. We perform the A-D test and obtain a standardized test statistic of  $T = 6.9807$  and  $p = 0.0006$ . Based on these values, we once again reject the null hypothesis at the  $\alpha = 0.01$  significance level. The results of these statistical tests strongly suggests that the two samples are *not* drawn from the same parent distribution.

The fact that the two samples appear to originate from separate parent distributions can be understood intuitively. The shorter period systems ( $P < 0.1$  d) will merge before they have a chance to cool to  $T_{\text{eff}} \lesssim 15,000$  K. On the other hand, the longer period binaries ( $P > 0.1$  d) have maximum merger times which are considerably longer and therefore they can survive long enough to cool below  $T_{\text{eff}} \lesssim 15,000$  K.

#### 4.2.3. The Future: Merger Products

In Figure 8 we plot the total minimum system mass (assuming  $i = 90^\circ$ ) as a function of the maximum merger time of the system. The maximum gravitational wave merger time is given by

$$\tau_{\text{merge,max}} = \frac{(M_1 + M_2)^{1/3}}{M_1 M_2} P^{8/3} \times 10^{-2} \text{Gyr} \quad (1)$$

where  $M_1$  is the mass of the ELM WD in  $M_\odot$ ,  $M_2$  is the minimum companion mass in  $M_\odot$ , and the period  $P$  is in hours (Landau & Lifshitz 1958).

Our new sample of 11 ELM WD binaries has yielded five new systems (J1054+2121, J1108+1512, J1130+3855, J1249+2626, J1526+0543) which are expected to merge within a Hubble time. Thus, the ELM Survey has now identified a total of 38 merger systems.

J0651 and WD 0931+444 remain the two shortest period systems, expected to merge in  $\approx 1$  Myr and  $\approx 10$  Myr, respectively. The most massive merger systems J1741+6526,

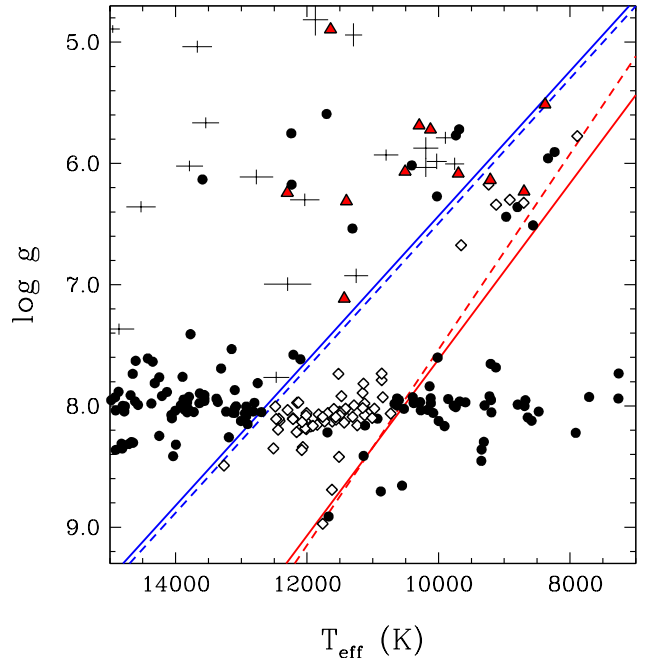


**Figure 10.** Region of the  $T_{\text{eff}} - \log g$  plane containing the canonical ZZ Ceti instability strip (lower left) and the six currently known ELM pulsators (upper right). All pulsators are identified as open diamonds, whereas WDs that have been confirmed as photometrically constant are represented as filled dots. The solid lines denote the blue and red boundaries from (Gianninas et al. 2014a). The blue and red dashed lines indicate the tentative new boundaries which take into account the 3D corrected values of  $T_{\text{eff}}$  and  $\log g$ . Error bars denote WDs from the ELM Survey sample which have not yet been investigated for photometric variability. Red triangles indicate the 11 new ELM WD binaries.

J0751–0141, near the top of Figure 8, represent potential Type Ia progenitors. However, the total mass of the system is not the only parameter that determines the ultimate fate of the binary. Marsh et al. (2004) showed that systems with high mass ratios will in fact lead to stable mass transfer binaries. In Figure 9 we plot the stability diagram from Marsh et al. (2004) and also plot the values of  $M_1$  and  $M_2$  for the entire ELM Survey sample for both the minimum and most likely (i.e. for  $i = 60^\circ$ ) companion mass. Note that in all cases, we choose  $M_2 > M_1$ .

As Kilic et al. (2014b) have shown, J1741+6526 and J0751–0141 are, given the uncertainties in  $M_2$ , located in the region of the stability diagram which predicts that they will eventually become stable mass transfer systems. Thus, they represent the progenitors of future AM CVn systems. However, Figure 9 also shows that two more ELM WD binaries lie this same region, namely J0811+0225 and J2132+0754. This brings the total to four unambiguous identifications of AM CVn progenitor systems. In addition, a number of systems do lie in the unstable regime, which predicts an eventual merger. However, the total mass for all of these merger systems is significantly below the Chandrasekhar mass.

Figure 9 also clearly shows that most ELM WD binaries are found in the regime between the stable and unstable regions. Indeed, there is still much uncertainty and debate over the eventual fate of compact double WD binaries. The recent calculations of Shen (2015) predict that most double WD binaries will eventually merge. On the other hand, Kremer et al. (2015) predict that a majority of systems will undergo stable mass transfer. Once the ELM Survey is com-

pleted, a more rigorous examination of both the Shen (2015) and Kremer et al. (2015) models will be possible by comparing these merging ELM WD binaries with the known populations of various merger products including AM CVn systems, R CrB stars and Type Ia supernovae.

#### 4.2.4. Instability Strip

The discovery of the first five pulsating ELM WDs were reported in Hermes et al. (2013a) and references therein. Recently, Kilic et al. (2015) discovered the sixth pulsating ELM WD which also happens to be the companion to PSR J1738+0333 (Antoniadis et al. 2012). These pulsating ELM WDs all have  $T_{\text{eff}} = 8000 - 10,000$  K and  $\log g = 6 - 7$  (see the updated instability strip in Figure 13 of Gianninas et al. 2014a). Furthermore, the location of this newly defined instability strip is in good agreement with the predictions of pulsation models (Van Grootel et al. 2013). In Figure 10 we plot an updated version of the figure from Gianninas et al. including the 11 new ELM WDs from this paper and the canonical ZZ Ceti instability strip (Gianninas et al. 2011) including several new discoveries presented by Green et al. (2015). One important difference here is that the adopted  $T_{\text{eff}}$  and  $\log g$  values for all the WDs in the figure have been corrected for 3D effects using the functions defined in Tremblay et al. (2013) for WDs with  $\log g > 7.0$  and Tremblay et al. (2015) for the ELM WD regime. In particular, the corrected atmospheric parameters for PSR J1738+0333 are  $T_{\text{eff}} = 8910 \pm 150$  K and  $\log g = 6.30 \pm 0.10$ .

Our best-fit temperatures and surface gravities place five of our new ELM WDs within (J1054–2121, J1108+1512) or near the blue edge (J0308+5140, J1130+3855, J1449+1717) of the instability strip as delineated by our new boundaries defined by Equations 2 and 3, respectively. Follow-up high-speed photometric observations of these five targets will be useful to search for pulsations in these ELM WDs and are under way with the McDonald 2.1m telescope (K. Bell 2015, private communication).

$$(\log g)_{\text{blue}} = 5.96923 \times 10^{-4}(T_{\text{eff}})_{\text{blue}} + 0.52431 \quad (2)$$

$$(\log g)_{\text{red}} = 8.06630 \times 10^{-4}(T_{\text{eff}})_{\text{red}} - 0.53039 \quad (3)$$

#### 4.2.5. Disk vs. Halo Membership

In Table 3 we list the ( $U$ ,  $V$ ,  $W$ ) space velocities for 49 of the 73 WDs from the ELM Survey for which proper motions were available from the SDSS+USNO-B catalog of Munn et al. (2004). In addition, the proper motion for J0345+1748 (NLTT 11748) is taken from Kawka & Vennes (2009) and its systemic velocity from Kilic et al. (2010a). Finally we adopt the proper motion from UCAC4 for J0308+5140.

We computed the ( $U$ ,  $V$ ,  $W$ ) space velocities and their associated uncertainties according to the prescription of Johnson & Soderblom (1987) combining the proper motions with our determinations of the systemic velocity (see Table 2). It is important to note that since we do not have parallax measurements for our targets, we adopt our spectroscopically determined distances as a proxy for the parallax. In addition, we correct for the motion of the local standard of rest using  $(U, V, W)_{\odot} = (11.10, 12.24, 7.25)$  km s<sup>-1</sup> as determined by Schönrich et al. (2010).

In Figure 11 we plot the  $W$  vs.  $V$  and  $U$  vs.  $V$  velocity distributions. In addition, we plot ellipsoids representing Galac-

**Table 3**  
Space Velocities of ELM WDs

SDSS	$U$ (km s <sup>-1</sup> )	$V$ (km s <sup>-1</sup> )	$W$ (km s <sup>-1</sup> )	$D_{\text{m,disk}}$	$D_{\text{m,halo}}$
J0022–1014	82 ± 23	–40 ± 21	27 ± 8	1.944	1.505
J0056–0611	–4 ± 7	–42 ± 9	–11 ± 3	0.520	1.376
J0106–1000	–126 ± 51	–236 ± 55	–16 ± 16	5.173	1.122
J0112+1835	67 ± 8	–104 ± 9	52 ± 8	2.677	1.055
J0152+0749	82 ± 12	–117 ± 19	–15 ± 13	2.597	0.812
J0345+1748	–147 ± 6	–197 ± 25	–28 ± 4	4.889	1.194
J0651+2844	–8 ± 4	2 ± 15	–9 ± 15	0.545	1.795
J0745+1949	–67 ± 4	–10 ± 4	23 ± 4	1.729	1.797
J0755+4800	–23 ± 3	25 ± 2	31 ± 3	1.440	2.053
J0815+2309	153 ± 19	–275 ± 38	–6 ± 25	6.037	1.270
J0822+2753	64 ± 6	–20 ± 9	–24 ± 7	1.434	1.622
J0825+1152	–71 ± 18	54 ± 24	–13 ± 24	2.217	2.359
J0849+0445	–20 ± 15	–20 ± 16	25 ± 17	0.957	1.630
J0900+0234	–8 ± 14	–52 ± 13	38 ± 14	1.363	1.368
J0917+4638	–25 ± 22	19 ± 32	9 ± 23	1.067	1.973
J0923+3028	11 ± 3	–16 ± 4	2 ± 3	0.231	1.618
J1046–0153	10 ± 6	–4 ± 7	–51 ± 6	1.427	1.797
J1053+5200	–112 ± 22	–201 ± 29	15 ± 13	4.440	0.947
J1056+6536	20 ± 22	–27 ± 24	20 ± 18	0.769	1.532
J1104+0918	–23 ± 3	–84 ± 6	31 ± 5	1.716	1.080
J1141+3850	280 ± 91	–345 ± 102	106 ± 32	9.378	2.664
J1234–0228	–2 ± 12	–70 ± 12	25 ± 6	1.292	1.157
J1238+1946	64 ± 47	–652 ± 65	–92 ± 9	12.952	4.492
J1422+4352	–48 ± 39	–72 ± 35	–165 ± 18	4.879	2.071
J1436+5010	43 ± 13	9 ± 12	–26 ± 8	1.228	1.871
J1443+1509	–33 ± 9	–167 ± 22	–141 ± 5	4.994	1.505
J1448+1342	6 ± 10	2 ± 11	–21 ± 7	0.687	1.795
J1512+2615	–5 ± 11	–60 ± 13	–5 ± 7	0.824	1.209
J1518+0658	–38 ± 4	–21 ± 5	–35 ± 3	1.288	1.645
J1538+0252	–179 ± 17	–126 ± 24	–1 ± 19	4.496	1.503
J1557+2823	26 ± 3	5 ± 3	17 ± 3	0.889	1.824
J1625+3632	56 ± 57	–136 ± 49	–22 ± 44	2.639	0.581
J1630+2712	36 ± 36	–91 ± 34	–106 ± 30	3.332	1.411
J1630+4233	34 ± 13	–8 ± 10	–10 ± 10	0.727	1.691
J1741+6526	39 ± 14	–55 ± 8	–14 ± 12	1.072	1.261
J1840+6423	118 ± 18	–61 ± 6	2 ± 12	2.617	1.389
J2132+0754	48 ± 14	–32 ± 10	–6 ± 13	0.993	1.474
J2228+3623	20 ± 5	–37 ± 5	26 ± 5	0.947	1.457
J2236+2232	–328 ± 33	–181 ± 11	–9 ± 13	7.903	2.447
J2338–2052	18 ± 22	11 ± 22	3 ± 8	0.702	1.868
J2345–0102	343 ± 35	–206 ± 26	69 ± 15	8.507	2.450
This paper					
J0308+5140	55 ± 1	–24 ± 2	12 ± 2	1.189	1.574
J0756+6704	17 ± 21	–227 ± 48	29 ± 24	4.244	0.523
J0837+6648	4 ± 7	–53 ± 10	8 ± 7	0.727	1.276
J1054–2121	8 ± 11	–64 ± 7	63 ± 9	2.080	1.369
J1108+1512	–29 ± 11	–40 ± 11	24 ± 6	1.121	1.454
J1130+3855	–85 ± 15	–29 ± 12	–1 ± 6	1.951	1.658
J1526+0543	21 ± 21	2 ± 27	–54 ± 19	1.575	1.855
J2151+1614	–53 ± 7	–44 ± 3	14 ± 5	1.405	1.452

tic thick-disk and stellar halo populations. We adopt average velocities of  $(\langle U \rangle, \langle V \rangle, \langle W \rangle) = (4, -20, -3)$  km s<sup>-1</sup> and  $(17, -187, -5)$  km s<sup>-1</sup>, and velocity dispersions of  $(\sigma_U, \sigma_V, \sigma_W) = (46, 50, 35)$  km s<sup>-1</sup> and  $(141, 106, 94)$  km s<sup>-1</sup> for the thick-disk and halo, respectively (Chiba & Beers 2000).

Treating the ellipsoids for the thick-disk and halo as mul-



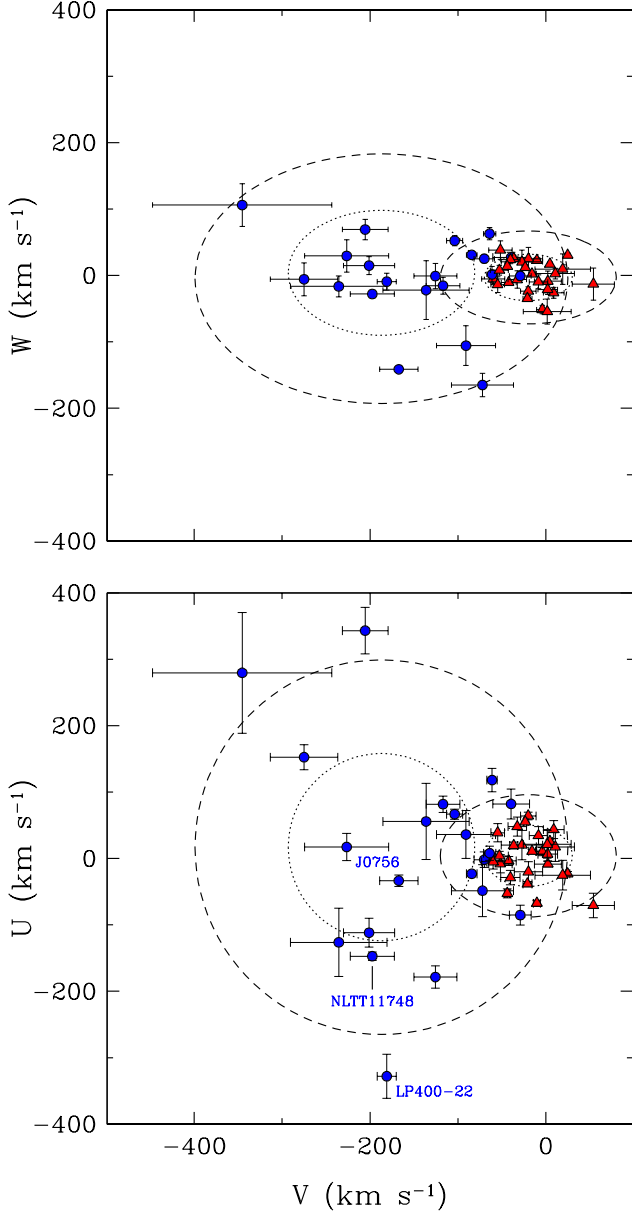


**Figure 11.**  $W$  vs.  $U$  (top) and  $U$  vs.  $V$  (bottom) velocity distributions for 49 ELM WD binaries including nine from this paper. Blue circles denote ELM WDs with a Mahalanobis distance suggesting halo membership while the red triangles represent ELM WDs with kinematics consistent with the Galactic thick-disk. The ellipsoids denote the  $1\text{-}\sigma$  (dotted) and  $2\text{-}\sigma$  (dashed) contours for Galactic thick-disk and stellar halo populations.

tivariate normal distributions, we compute the Mahalanobis distance, as defined in Equation (4), for each ELM WD. This measures the distance from the center of the distributions in units of standard deviations and provides a quantitative indicator of group membership.

$$D_m = \sqrt{\frac{(U - \langle U \rangle)^2}{\sigma_U^2} + \frac{(V - \langle V \rangle)^2}{\sigma_V^2} + \frac{(W - \langle W \rangle)^2}{\sigma_W^2}} \quad (4)$$

The Mahalanobis distances with respect to the thick-disk and halo distributions,  $D_{m,\text{disk}}$  and  $D_{m,\text{halo}}$ , are listed in Table 3. Based on these values, 27 ELM WDs have distances consistent with disk membership while the remaining 22 WDs have distances consistent with halo membership. J0756+6704, the

ELM WD with the most negative systemic velocity among the 11 new ELM WD binaries, numbers among the likely halo members. Unsurprisingly, LP 400-22 (J2236+2232) also stands out in the bottom panel of Figure 11 with  $U = -332 \text{ km s}^{-1}$ . The case of LP 400-22 is well documented (Kawka et al. 2006; Vennes et al. 2009; Kilic et al. 2013) and the results here serve only to further confirm that LP 400-22 is indeed a unique member of the halo. We also find that NLTT 11748 is a halo object, in agreement with Kawka & Vennes (2009) and Kilic et al. (2010a).

The breakdown of halo versus thick-disk members suggests that  $\approx 40\%$  of the WDs from the ELM Survey are members of the Galactic halo. However, this result is based solely on a kinematic metric. Additional considerations, such as the location of the ELM WDs versus the scale height of the disk, may provide additional information not considered here. As such, we suggest that our result represents an upper limit for the percentage of halo objects in the ELM Survey.

Having said that, the fact that our sample includes a significant fraction of halo stars should not be unexpected. This result is most likely a logical consequence of our candidates being largely selected from the SDSS which is a high Galactic latitude survey. Given the luminosity of our targets, our apparent magnitude range samples white dwarfs in the range  $0.1 \lesssim |Z| \lesssim 2 \text{ kpc}$ , where  $Z$  denotes the vertical distance from the Galactic plane. Given the scale height of the disk and the relative normalization of the disk and halo, it is not surprising that the ELM Survey contains a significant number of halo stars.

## 5. CONCLUSIONS

We present radial velocity measurements and stellar atmosphere fits for 11 new ELM WD binaries with  $P < 1 \text{ d}$ . This brings the total of ELM WDs identified by the ELM Survey up to 73 demonstrating the continued effectiveness of using SDSS colors to identify ELM WD candidates. Based on our optical spectra, we perform spectroscopic fits, compute orbital solutions, and provide a complete set of physical and binary parameters for each system.

We review the recent evolutionary calculations of Istrate et al. (2014) and compare them to the existing models of Althaus et al. (2013). There are significant differences between the two sets of evolutionary models. These can be traced back to the different initial assumptions made about the nature and composition of the progenitor binaries. We can only conclude that there still remains much uncertainty regarding the exact evolutionary history of ELM WDs and additional modeling is required to form a coherent picture. Thankfully, the systematic uncertainty when deriving masses from the independent model sets is only  $\approx 0.01 M_\odot$ .

When considering the distribution of orbital periods as a function of  $T_{\text{eff}}$ , we have shown that two distinct populations are emerging. The shorter period systems are generally found with  $T_{\text{eff}} > 15,000 \text{ K}$  while the longer period systems can cool to much lower  $T_{\text{eff}}$ .

Of the 11 new ELM WD binaries, five will merge within a Hubble time. Unfortunately, the final merger product for the majority of ELM WD binaries remains uncertain. Nonetheless, we have identified four systems which will undergo stable mass transfer and ultimately become AM CVn systems.

Based on our updated boundaries of the instability strip, we have also identified a number of potentially interesting targets for follow-up high-speed photometric observations. These ELM WDs have atmospheric parameters within or near the

instability strip of pulsating ELM WDs, an extension of the canonical ZZ Ceti instability strip.

Finally, a study of the kinematics of ELM WDs reveals that the majority of these binaries are members of the Galactic disk. However, a non-negligible fraction of ELM WDs are most certainly members of the Galactic halo, a result of our reliance on SDSS colors to identify candidates.

We would like to thank the referee and statistics consultant for their useful suggestions which helped improve this paper. We also thank the director and staff of Kitt Peak National Observatory for the use of their facilities and their valuable assistance. We gratefully acknowledge the support of the NSF under grant AST-1312678, and NASA under grant NNX14AF65G. This work was supported in part by National Science Foundation Grant No. PHYS-1066293 and the hospitality of the Aspen Center for Physics. AG acknowledges support provided by NASA through grant number HST-GO-13319.01 from the Space Telescope Science Institute, which is operated by AURA, Inc., under NASA contract NAS 5-26555. This material is based upon work supported by AURA through the National Science Foundation under AURA Cooperative Agreement AST 0132798 as amended.

*Facilities:* MMT (Blue Channel Spectrograph), KPNO 4m telescope (RCSpec, KOSMOS), Palomar Hale 5m telescope (Double Spec), FWLO 1.5m telescope (FAST)

## APPENDIX

### ELM WD PARAMETERS

We provide in Tables 4 and 5 a complete listing of the physical and binary parameters for the entire ELM Survey sample. This includes the 62 ELM WDs from previous publications as well as the 11 new ELM WDs presented here. We note that for ELM WDs with  $T_{\text{eff}} < 12,000$  K, the atmospheric parameters have been adjusted using the 3D corrections from Tremblay et al. (2015). We also note that we have updated our value of the apparent magnitude for J0345+1748 (NLTT 11748). In Gianninas et al. (2014b) we had adopted the value of  $V = 16.5$  from Kawka & Vennes (2009). We now adopt the value of  $g = 16.797$  from UCAC4. We then take  $A_g/E(B-V) = 3.793$  from IRSA and  $E(B-V) = 0.10$  from Kawka & Vennes (2009) to obtain an extinction of  $A_g = 0.3793$ . Thus, our final extinction-corrected  $g$ -band magnitude for NLTT 11748 is  $g_0 = 16.418$ .

### DATA TABLE

Table 6 presents our radial velocity measurements for the 11 new ELM WD binaries presented here. The table columns include object name, heliocentric Julian date, heliocentric radial velocity, and velocity error.

## REFERENCES

- Althaus, L. G., Miller Bertolami, M. M., & Córscico, A. H. 2013, *A&A*, 557, A19
- Amaro-Seoane, P., Aoudia, S., Babak, S., et al. 2012, *Classical and Quantum Gravity*, 29, 124016
- Andrews, J. J., Price-Whelan, A. M., & Agüeros, M. A. 2014, *ApJL*, 797, L32
- Antoniadis, J., van Kerkwijk, M. H., Koester, D., et al. 2012, *MNRAS*, 423, 3316
- Bildsten, L., Shen, K. J., Weinberg, N. N., & Nelemans, G. 2007, *ApJL*, 662, L95
- Boffin, H. M. J. 2015, *A&A*, 575, L13
- Brown, J. M., Kilic, M., Brown, W. R., & Kenyon, S. J. 2011a, *ApJ*, 730, 67
- Brown, W. R., Kilic, M., Allende Prieto, C., Gianninas, A., & Kenyon, S. J. 2013, *ApJ*, 769, 66
- Brown, W. R., Kilic, M., Allende Prieto, C., & Kenyon, S. J. 2010, *ApJ*, 723, 1072
- . 2012, *ApJ*, 744, 142
- Brown, W. R., Kilic, M., Hermes, J. J., et al. 2011b, *ApJL*, 737, L23
- Chiba, M., & Beers, T. C. 2000, *AJ*, 119, 2843
- Clayton, G. C. 2013, in *Astronomical Society of the Pacific Conference Series*, Vol. 469, 18th European White Dwarf Workshop., ed. Krzesiñ, J. ski, G. Stachowski, P. Moskalik, & K. Bajan, 133
- Cui, X.-Q., Zhao, Y.-H., Chu, Y.-Q., et al. 2012, *Research in Astronomy and Astrophysics*, 12, 1197
- Debes, J. H., Kilic, M., Tremblay, P.-E., et al. 2015, *AJ*, 149, 176
- Fabricant, D., Cheimets, P., Caldwell, N., & Geary, J. 1998, *PASP*, 110, 79
- Foley, R. J. 2015, *ArXiv e-prints*, arXiv:1501.07607
- Gianninas, A., Bergeron, P., & Ruiz, M. T. 2011, *ApJ*, 743, 138
- Gianninas, A., Dufour, P., Kilic, M., et al. 2014a, *ApJ*, 794, 35
- Gianninas, A., Hermes, J. J., Brown, W. R., et al. 2014b, *ApJ*, 781, 104
- Green, E. M., Limoges, M.-M., Gianninas, A., et al. 2015, in *Astronomical Society of the Pacific Conference Series*, Vol. 493, 19th European Workshop on White Dwarfs, ed. P. Dufour, P. Bergeron, & G. Fontaine, 237
- Hallakoun, N., Maoz, D., Kilic, M., et al. 2015, *ArXiv e-prints*, arXiv:1507.06311
- Hansen, B. M. S., Anderson, J., Brewer, J., et al. 2007, *ApJ*, 671, 380
- Hermes, J. J., Montgomery, M. H., Gianninas, A., et al. 2013a, *MNRAS*, 436, 3573
- Hermes, J. J., Montgomery, M. H., Winget, D. E., et al. 2013b, *ApJ*, 765, 102
- Hermes, J. J., Brown, W. R., Kilic, M., et al. 2014, *ApJ*, 792, 39
- Iben, Jr., I., & Tutukov, A. V. 1984, *ApJS*, 54, 335
- Istrate, A. G., Tauris, T. M., Langer, N., & Antoniadis, J. 2014, *A&A*, 571, L3
- Johnson, D. R. H., & Soderblom, D. R. 1987, *AJ*, 93, 864
- Kawka, A., & Vennes, S. 2009, *A&A*, 506, L25
- Kawka, A., Vennes, S., Oswalt, T. D., Smith, J. A., & Silvestri, N. M. 2006, *ApJL*, 643, L123
- Kenyon, S. J., & Garcia, M. R. 1986, *AJ*, 91, 125
- Kilic, M., Allende Prieto, C., Brown, W. R., et al. 2010a, *ApJL*, 721, L158
- Kilic, M., Brown, W. R., Allende Prieto, C., et al. 2011, *ApJ*, 727, 3
- . 2012, *ApJ*, 751, 141
- Kilic, M., Brown, W. R., Allende Prieto, C., Kenyon, S. J., & Pani, J. A. 2010b, *ApJ*, 716, 122
- Kilic, M., Brown, W. R., Gianninas, A., et al. 2014a, *MNRAS*, 444, L1
- Kilic, M., Hermes, J. J., Gianninas, A., & Brown, W. R. 2015, *MNRAS*, 446, L26
- Kilic, M., Gianninas, A., Brown, W. R., et al. 2013, *MNRAS*, 434, 3582
- Kilic, M., Hermes, J. J., Gianninas, A., et al. 2014b, *MNRAS*, 438, L26
- Kremer, K., Sepinsky, J., & Kalogera, V. 2015, *ApJ*, 806, 76
- Kurtz, M. J., & Mink, D. J. 1998, *PASP*, 110, 934
- Landau, L. D., & Lifshitz, E. M. 1958, *The Classical Theory of Fields* (Oxford: Pergamon Press)
- Liebert, J., Bergeron, P., & Holberg, J. B. 2005, *ApJS*, 156, 47
- Marsh, T. R., Dhillon, V. S., & Duck, S. R. 1995, *MNRAS*, 275, 828
- Marsh, T. R., Nelemans, G., & Steeghs, D. 2004, *MNRAS*, 350, 113
- Martini, P., Elias, J., Points, S., et al. 2014, in *Society of Photo-Optical Instrumentation Engineers (SPIE) Conference Series*, Vol. 9147, Society of Photo-Optical Instrumentation Engineers (SPIE) Conference Series, 91470Z
- Massey, P., Strobel, K., Barnes, J. V., & Anderson, E. 1988, *ApJ*, 328, 315
- Moran, C., Marsh, T. R., & Bragaglia, A. 1997, *MNRAS*, 288, 538
- Munn, J. A., Monet, D. G., Levine, S. E., et al. 2004, *AJ*, 127, 3034
- Napiwotzki, R., Karl, C. A., Nelemans, G., et al. 2007, in *Astronomical Society of the Pacific Conference Series*, Vol. 372, 15th European Workshop on White Dwarfs, ed. R. Napiwotzki & M. R. Burleigh, 387
- Nelson, L. A., Dubeau, E., & MacCannell, K. A. 2004, *ApJ*, 616, 1124
- Oke, J. B., & Gunn, J. E. 1982, *PASP*, 94, 586
- Parsons, S. G., Marsh, T. R., Gänsicke, B. T., Drake, A. J., & Koester, D. 2011, *ApJL*, 735, L30
- Perets, H. B., Gal-Yam, A., Mazzali, P. A., et al. 2010, *Nature*, 465, 322
- Press, W. H., Flannery, B. P., & Teukolsky, S. A. 1986, *Numerical recipes. The art of scientific computing*
- Schmidt, G. D., Weymann, R. J., & Foltz, C. B. 1989, *PASP*, 101, 713

**Table 4**  
ELM WD Physical Parameters

SDSS	$T_{\text{eff}}$ (K)	$\log g$ ( $\text{cm s}^{-2}$ )	$M_1$ ( $M_{\odot}$ )	Radius ( $R_{\odot}$ )	$g_0$ (mag)	$M_g$ (mag)	$d$ (kpc)	$\tau_{\text{cool}}$ (Gyr)
J0022+0031	20460 $\pm$ 310	7.58 $\pm$ 0.05	0.457 $\pm$ 0.016	0.0182 $\pm$ 0.0013	19.284 $\pm$ 0.033	9.84 $\pm$ 0.18	0.774 $\pm$ 0.065	0.215 $\pm$ 0.128
J0022-1014	20730 $\pm$ 340	7.28 $\pm$ 0.05	0.375 $\pm$ 0.016	0.0233 $\pm$ 0.0018	19.581 $\pm$ 0.031	9.28 $\pm$ 0.20	1.151 $\pm$ 0.107	0.042 $\pm$ 0.021
J0056-0611	12240 $\pm$ 180	6.18 $\pm$ 0.04	0.174 $\pm$ 0.010	0.0564 $\pm$ 0.0045	17.208 $\pm$ 0.023	8.37 $\pm$ 0.21	0.585 $\pm$ 0.056	0.957 $\pm$ 0.081
J0106-1000	16970 $\pm$ 260	6.10 $\pm$ 0.05	0.191 $\pm$ 0.010	0.0642 $\pm$ 0.0051	19.595 $\pm$ 0.023	7.45 $\pm$ 0.20	2.691 $\pm$ 0.253	0.497 $\pm$ 0.168
J0112+1835	9740 $\pm$ 140	5.77 $\pm$ 0.05	0.160 $\pm$ 0.010	0.0863 $\pm$ 0.0080	17.110 $\pm$ 0.016	8.01 $\pm$ 0.25	0.662 $\pm$ 0.077	1.822 $\pm$ 0.196
J0152+0749	10800 $\pm$ 180	5.93 $\pm$ 0.05	0.168 $\pm$ 0.010	0.0736 $\pm$ 0.0061	18.033 $\pm$ 0.009	8.08 $\pm$ 0.22	0.980 $\pm$ 0.102	1.407 $\pm$ 0.137

(This table is available in its entirety in a machine-readable form in the online journal. A portion is shown here for guidance regarding its form and content.)

**Table 5**  
ELM WD Binary Parameters

SDSS	$P$ (days)	$K$ ( $\text{km s}^{-1}$ )	Mass Function ( $M_{\odot}$ )	$M_2$ ( $M_{\odot}$ )	$M_{2,i=60^{\circ}}$ ( $M_{\odot}$ )	$\tau_{\text{merge}}$ (Gyr)	$a$ ( $R_{\odot}$ )	$\log h$
J0022+0031	0.49135 $\pm$ 0.02540	80.8 $\pm$ 1.3	0.027 $\pm$ 0.003	$\geq$ 0.23 $\pm$ 0.02	0.28 $\pm$ 0.02	...	2.32 $\pm$ 0.11	-22.79
J0022-1014	0.07989 $\pm$ 0.00300	145.6 $\pm$ 5.6	0.026 $\pm$ 0.004	$\geq$ 0.21 $\pm$ 0.02	0.25 $\pm$ 0.02	$\leq$ 0.616	0.65 $\pm$ 0.03	-22.55
J0056-0611	0.04338 $\pm$ 0.00002	376.9 $\pm$ 2.4	0.241 $\pm$ 0.005	$\geq$ 0.46 $\pm$ 0.02	0.61 $\pm$ 0.02	$\leq$ 0.120	0.45 $\pm$ 0.01	-22.06
J0106-1000	0.02715 $\pm$ 0.00002	395.2 $\pm$ 3.6	0.174 $\pm$ 0.005	$\geq$ 0.39 $\pm$ 0.02	0.51 $\pm$ 0.02	$\leq$ 0.036	0.32 $\pm$ 0.01	-22.61
J0112+1835	0.14698 $\pm$ 0.00003	295.3 $\pm$ 2.0	0.392 $\pm$ 0.008	$\geq$ 0.62 $\pm$ 0.02	0.85 $\pm$ 0.03	$\leq$ 2.682	1.08 $\pm$ 0.01	-22.40
J0152+0749	0.32288 $\pm$ 0.00014	217.0 $\pm$ 2.0	0.342 $\pm$ 0.010	$\geq$ 0.57 $\pm$ 0.02	0.78 $\pm$ 0.03	...	1.79 $\pm$ 0.03	-22.80

(This table is available in its entirety in a machine-readable form in the online journal. A portion is shown here for guidance regarding its form and content.)

**Table 6**  
Radial Velocity Measurements

Object	HJD (days - 2455000)	$v_{\text{helio}}$ ( $\text{km s}^{-1}$ )
J0308+5140	1634.76726	19.2 $\pm$ 13.6
...	1716.63827	-145.6 $\pm$ 19.9
...	1716.64861	-132.3 $\pm$ 22.6
...	1716.65891	-154.4 $\pm$ 22.8
...	1716.66922	-134.4 $\pm$ 26.4
...	1946.81093	9.7 $\pm$ 12.1

(This table is available in its entirety in a machine-readable form in the online journal. A portion is shown here for guidance regarding its form and content.)

- Schönrich, R., Binney, J., & Dehnen, W. 2010, MNRAS, 403, 1829  
 Seaton, M. J. 1979, MNRAS, 187, 73P  
 Shen, K. J. 2015, ApJL, 805, L6  
 Shporer, A., Kaplan, D. L., Steinfadt, J. D. R., et al. 2010, ApJL, 725, L200  
 Solheim, J.-E. 2010, PASP, 122, 1133  
 Steinfadt, J. D. R., Kaplan, D. L., Shporer, A., Bildsten, L., & Howell, S. B. 2010, ApJL, 716, L146  
 Tremblay, P.-E., & Bergeron, P. 2009, ApJ, 696, 1755  
 Tremblay, P.-E., Gianninas, A., Kilic, M., et al. 2015, ApJ, 809, 148  
 Tremblay, P.-E., Ludwig, H.-G., Steffen, M., & Freytag, B. 2013, A&A, 559, A104  
 Van Grootel, V., Fontaine, G., Brassard, P., & Dupret, M.-A. 2013, ApJ, 762, 57  
 Vennes, S., Kawka, A., Vaccaro, T. R., & Silvestri, N. M. 2009, A&A, 507, 1613  
 Vennes, S., Thorstensen, J. R., Kawka, A., et al. 2011, ApJL, 737, L16  
 Wang, S.-G., Su, D.-Q., Chu, Y.-Q., Cui, X., & Wang, Y.-N. 1996, Appl. Opt., 35, 5155  
 Webbink, R. F. 1984, ApJ, 277, 355  
 Zacharias, N., Finch, C. T., Girard, T. M., et al. 2013, AJ, 145, 44  
 Zhao, J. K., Luo, A. L., Oswalt, T. D., & Zhao, G. 2013, AJ, 145, 169